International Journal of Signal Processing, Image Processing and Pattern Recognition
Vol.9, No.7 (2016), pp.203-212
http://dx.doi.org/10.14257/ijsip.2016.9.7.17

# Dual Focusing Ultrasonic Imaging Algorithm Based on Chirp-Coded and Adaptive Beamforming Combination

WANG Linhong[1],Gao Yang[2] , Li Na[2] and YU Tiezhu[3]

[1]*Institute of Applied Electronics, Chongqing College of Electronic Engineering, Chongqing, China*
[2]*State Key Laboratory of Power Transmission Equipment & System Security and New Technology, Chongqing University Chongqing, China*
[3]*Daewoo Cutting &Welding Equipment (Yan Tai) CO., LTD., Yantai China*
*cqbj2005@126.com*

***Abstract***

*According to the inherent deficiency of traditional beamformer on anti-noise and lateral resolution, this paper proposes a method based on the combination of Chirp-coded and adaptive dual focusing beamformer (CARDFB). Firstly, Chirp-coded technology is introduced to improve the transmitting average power, and then the dual focusing beamformer and adaptive beamformer are combined to obtain a higher quality beamforming signal. Finally, the signal filtered with matched filter is used for imaging. Experimental results indicate that the proposed CARDFB algorithm can achieve higher lateral resolution, better main-to-side lobe ratio and are more robust to noise compared with traditional dynamic focusing combined with adaptive focusing beamformer.*

***Keywords:*** *We would like to encourage you to list your keywords in this section*

## 1. Introduction

Beamforming is an important part of ultrasound imaging system. The traditional delay and sum (DAS) algorithm is easy to achieve. However, its poor performance of lateral resolution, signal-to-noise ratio (SNR) and imaging contrast cannot meet the requirement in many occasions [1]. Ref. [2-4] introduce coded excitation to improve the imaging contrast, vertical resolution and robustness to noise, however, the coded excitation is ineffective to improve the lateral resolution. Recently, virtual source element [5-8] and adaptive beamforming algorithm [9-11] are widely used in sonar detection and ultrasound imaging systems. Virtual source technology can improve the lateral resolution of the image and deepen the investigation depth by increasing the number of array elements in virtual to widen the receiving aperture. However, the application of virtual elements always increases the sidelobe and the artifacts that will decrease the overall quality of the ultrasound image.

To solve this problem, a method combining the adaptive algorithm with virtual element technique is proposed. The adaptive filter [11-13] is introduced to process the echo signal received by the virtual element, which can effectively suppress the sidelobe and artifacts; however, its performance of robustness and the axial resolution cannot be improved.

According to the advantages of the above algorithms, a combination method based on Chirp-coded and adaptive robust dual focusing beamformer is proposed in this paper. To investigate the effectiveness of the proposed method, the experiments of static-scatter targets imaging are conducted.

The basic theory of Chirp-coded excitation, pulse compression and adaptive algorithm are descripted in Section II. The Chirp-coded, adaptive robust dual focusing beamforming

ISSN: 2005-4254 IJSIP

algorithm is illustrated in Section III. The investigation of the proposed method with experiments are conducted in Section IV and the conclusion is drawn in Section V.

## 2. Chirp-Coded Excitation Theory and Adaptive Weighting Algorithm

### 2.1. Chirp-Coded Excitation and Pulse Compression

Chirp-coded signal is widely used in radar system, and its complex expression is given by

$$p(t)=\alpha(t)\bullet\exp\left\{j2\pi\left[\left(f_0-\frac{B}{2}\right)t+\frac{B}{2T}t^2\right]\right\},0\le t\le T \tag{1}$$

where $\alpha(t)$ is the amplitude, $f_0$ is the central frequency, $T$ is the total duration and $B$ is the bandwidth.

The compression ratio (CR) of Chirp signal can be defined as $CR=TB$. When the bandwidth $B$ is constant, the CR will change with the duration. However, the Chirp-coded excitation can not improve the lateral resolution of the ultrasound imaging.

The pulse compression is performed with matched filter at the receiver. For the echo signal without attenuation, the matched filter is the autocorrelation of the signal. If $\alpha(t)$ in Equation (1) is a rectangle signal rect($t/T$), then the output signal of the matched filter is

$$R_{pp}(\tau)=\int_{-\infty}^{\infty}p(t)p^*(t+\tau)\mathrm{d}t=T\frac{\sin\left[\pi Y\frac{\tau}{T}\left(1-\frac{\tau}{T}\right)\right]}{\pi Y\frac{\tau}{T}}e^{-j2\pi f_0\tau} \tag{2}$$

where $Y=CR$.

The output signal of the matched filter approximates the impulse function that diminishes the frequency modulation, but the sidelobe remains high.

### 2.2. Adaptive Weighting Algorithm

For a equally-spaced $M$ elements, some point-scattering targets are in near field. The output of the beamformer is

$$y(k)=\boldsymbol{w}^H(k)X_d(k)=\sum_{i=1}^{M}w_i(k)x_i(k-\Delta_i) \tag{3}$$

where $k$ is the sequence number, $\boldsymbol{X}_d(k)=[x_1(k-\square_\square),\ldots,x_M(k-\square_\square)]^T$ is the focusing delay, $\boldsymbol{w}(k)=[w_1(k),\ldots,w_M(k)]^T$ is the weighting vector, $\square_i$ is the delay of each channel. If $\boldsymbol{w}(k)$ is a unit vector, Equation (3) is the traditional delay and sum algorithm (DAS). When $\boldsymbol{w}(k)$ is real-timely calculated from the received data, Equation (3) is the adaptive beamforming algorithm.

The Capon algorithm is the most widely used method in adaptive beamforming which can be expressed by [14]

$$\min_{\boldsymbol{w}}\boldsymbol{w}^H\boldsymbol{R}_{i+n}\boldsymbol{w},\ subject\quad to\quad \boldsymbol{w}^H\boldsymbol{a}=1 \tag{4}$$

where $\boldsymbol{w}$ is the optimal weighting vector needed to be solved, $\boldsymbol{R}_{i+n}$ is a $M\times M$ spatial covariance matrix, $\boldsymbol{a}$ is the steering vector. By using the Lagrange multiplier, the solution to (4) is given by

$$\boldsymbol{w}_{\mathrm{opt}}=\frac{\boldsymbol{R}_{\mathrm{i+n}}^{-1}\boldsymbol{a}}{\boldsymbol{a}^{\mathrm{H}}\boldsymbol{R}_{\mathrm{i+n}}^{-1}\boldsymbol{a}} \tag{5}$$

 

In fact, the exact $\boldsymbol{R}_{i+n}$ cannot be obtained and should be estimated as accurate as possible. In general, $\boldsymbol{R}_{i+n}$ in Equation (5) is estimated through spatial smoothing method [15-16] and it can be represented as

$$\tilde{\boldsymbol{R}} = \frac{1}{M-L+1} \sum_{l=1}^{M-L+1} X_d^l(k)[\mathrm{X}_d^l(k)]^{\mathrm{H}} \tag{6}$$

where $L$ is the subarray number, $X_d^l(k) = [x_d^l(k), x_d^{l+1}(k), \ldots, x_d^{l+L-1}(k)]$ is the output vector, $[\cdot]^{\mathrm{H}}$ is the conjugate transpose of $[\cdot]$. Actually, $\tilde{\boldsymbol{R}}$ is a sample covariance matrix.

## 3. Chirp-Coded Adaptive Robust Dual Focusing Beamforming

The Chirp-coded adpative robust dual focusing beamforming (CARDFB) consists of two beamforming stages and a memory for storing the intermediate data from the first beamforming stage (BF1). Chirp-coded excitation is applied in the first part. The virtural element (VE) acts as a focus for transmitting and receiving [17]. The first stage is conducted by BF1 with echo signals receiving from channels. The output data of BF1 are stored in the FIFO buffer. In the second stage, the adaptive weighting vector is real-timely obtained according to the data read from FIFO buffer, and then the adaptive beamforming is conducted by BF2. After the second focusing, the pulse compressing is conducted. At last the data for imaging is obtained. The scheme of CARDFB is shown in Figure.1.

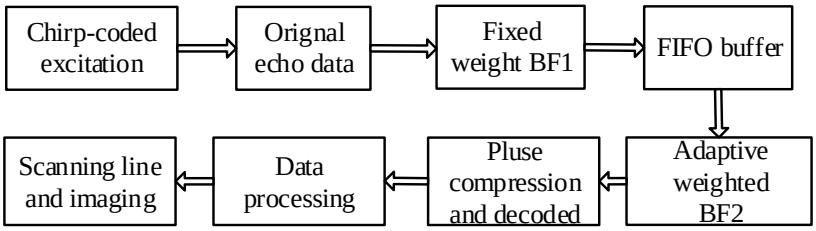


**Figure 1. Schematic Diagram of CARDFB**

### 3.1. The First Beamformer (BF1)

The first beamforming stage is to construct and store a set of focusing lines by sliding the sub-aperture. These 1st stage lines are obtained with a single focal point in both transmitting and receiving process. The transmitting focal point is considered as a virtual source (VS). BF1 has a fixed receiving focus and this focal point is considered as a virtual receiver (VR). When the VS and the VR coincide, the focal points can be considered as a virtual transducer element (VE). The process of obtaining the scanning line in BF1 stage is shown in Figure 2 (a). Figure 2 (b) shows the delay calculation of BF1.

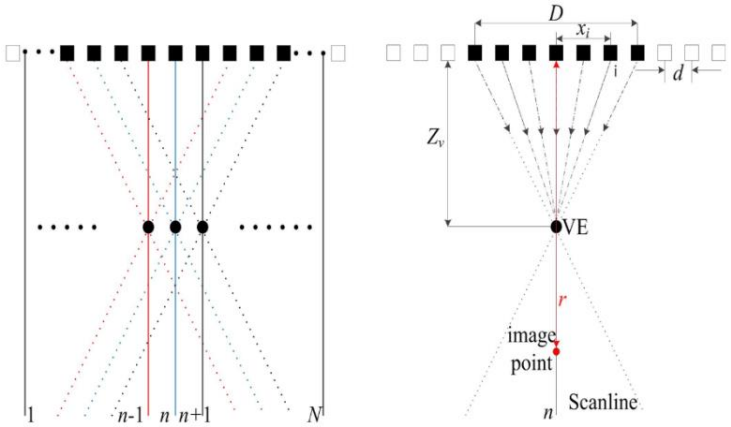


(a) Generation of scanning line (b) Delay calculation

**Figure 2. Generation of Scanning Line and Delay Calculation of BF1**

In Figure 2(b), $d$ is the pitch width, $Z_v$ is the depth of virtual element, $F\#$ is F-number, the number of the linear sub-aperture is $L=Z_v/F\#/d$[17], $D=L\times d$ is the size of the sub-aperture. Set the center of the sub-apertures as reference points, then $x_i$ and $\tau_i$ of the $i$-*th* sub-aperture can be calculated from Equation (7):

$$\begin{cases} x_i = \left( i - \dfrac{L+1}{2} \right) \cdot d, \quad i = 1, 2, ..., L \\ \tau_i = \dfrac{\sqrt{x_i^2 + Z_v^2} - Z_v}{c} \end{cases} \tag{7}$$

The $n$-th scanning line $S_n(t)$ can be obtained as:

$$\begin{cases} S_n(t) = \sum_{i=1}^{L} W_{BF1}(i)\, s_i\left( t - \dfrac{r}{c} - \tau_i \right) \\ W_{BF1}(i) = 0.5\left[ 1 - \cos\left( 2\pi \dfrac{i}{L} \right) \right], 0 \le i \le L \end{cases} \tag{8}$$

where $W_{BF1}$ is a dynamic apodization function, in this work we choose Hanning window, which can suppress the effect of sidelobe. $s_i(t)$ is the receiving signal from the $i$-th sub-aperture. $r/c$ is the transmitting time from target point to the center of sub-aperture, $\tau_i$ is the delay value.

### 3.2. The Second Beamformer (BF2)

In general, a single image point is represented in multiple BF1 image lines obtained from multiple emissions. This is exploited in BF2, where each of sample is constructed by selecting a sample from each of those output lines from BF1, which contain information from the spatial position of the image points and summing a weighted set of these samples. When multiple virtual elements exist simultaneously, the acoustic field will superpose. Equation (9) shows the method for confirming whether a sample *ii* is in the acoustic field of virtual element *jj* [18-19].

$$K_{jj,ii} = \begin{cases} 1, & if \left| d\_x / d\_z \right| \le \tan\theta_a \\ 0, & if \left| d\_x / d\_z \right| > \tan\theta_a \end{cases} \tag{9}$$

where $d\_x$ is the lateral distance between the sample point and the corresponding virtual element, $d\_z$ is the axial distance, $\theta_a$ is the half aperture angle. $K_{jj,ii}=1$ indicates the sample is inside the acoustic field of the virtual element, and it's an effective sample. The delay of any sample point *ii* to virtual element *jj* is expressed as

$$\tau_{jj,ii} = 2\,\frac{Z_v \pm \sqrt{d\_x^2 + d\_z^2}}{c} \tag{10}$$

where "$\pm$" refer to whether the image point is above or below the corresponding virtual element. The half aperture angle $\theta_a$ can be obtained by

$$\theta_a = \arctan\frac{D}{2Z_v} = \arctan\frac{1}{2F\#} \tag{11}$$

The geometric relationship between $\theta_a$ and virtual element is shown in Figure 3.

 

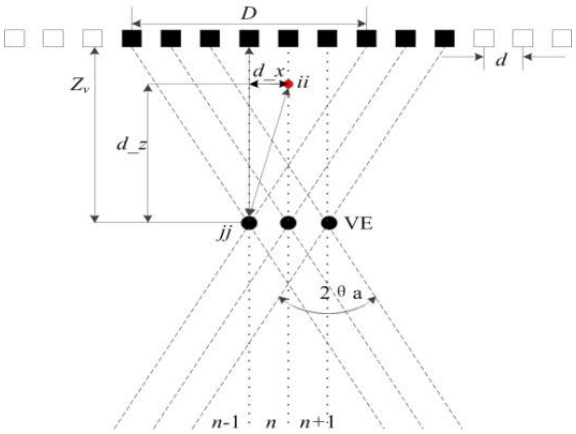


**Figure 3. Diagram of Half Aperture $\theta_a$ and Delay Calculation of BF2**

In the second stage, point-by-point focusing beamforming is adopted. The delay of other points can be calculated with Equation (11). The data of number *n* scanning line from BF2 is

$$H_{n,ii}(t)=\sum_{jj=1}^{N}W_{BF2}(jj)K_{jj,ii}S_{jj,ii}\left(t-\tau_{jj,ii}\right),\quad ii=1,2,...,M \tag{12}$$

where $W_{BF2}=w_{opt}$ is the corresponding adaptive weight, $M$ is the number of total sample points, $N$ is the number of scanning line of BF1, $S_{jj,ii}(t)$ is the signal of number $ii$ sample point on the number $jj$ scanning line of BF1. $\tau_{jj,ii}$ is the delay of point $ii$ relative to number $jj$ VE.

## 4. Experimental Results

The proposed CARDFB method is investigated in Field II [20]. The images of point targets are obtained by different beamforming algorithms. The axial and lateral resolution and robustness are extracted and compared to the traditional beamforming algorithms, such as dynamic receive focusing (DRF), adaptive beamforming (AB) [14] , dual focusing beamforming (DFB) [18] and dual focusing adaptive beamforming (DFAB) [14-18].

In the experiment, the fixed point transmitting and dynamic receiving focusing are employed. The element number of the linear array is $N$=128. The center frequency of transmitting signal is 3.5MHz, the sampling frequency is 50MHz, the pitch is $d$=0.48mm and the speed of ultrasound is c=1540m/s. The dynamic range of images are normalized from -40dB to 0dB.

For DFB, DFAB and CARDFB methods, the depth of VE is $Z_v$=20mm. The F-number $F\#$=2. For CARDFB algorithm, the center frequency of Chirp signal is 3.5MHz, the fractional bandwidth is 80% and the duration of the Chirp code is 10μs.

### 4.1. Resolution Investigation

There are 16-point targets distributed within the depth from 60mm to 95mm and 16mm width, the axial interval is 5mm, and the lateral interval is 2mm. The simulation results with different methods are shown in Figure 4(a) and the comparison of lateral curves at the depth of 85mm are shown in Figure 4(b).

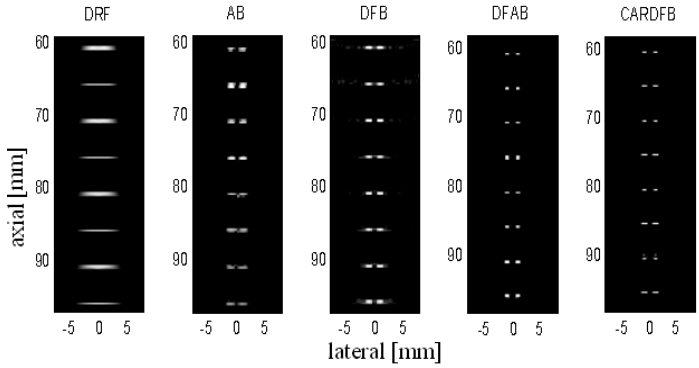


(a)Images of point targets using different beamforming methods

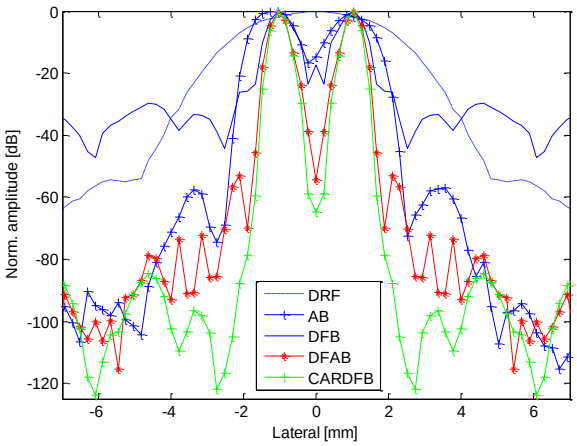


(b) The comparison of lateral curvls at the depth of 85mm

**Figure 4. Simulation Comparison of Different Beamforming Methods**

As can be seen from Figure 4(a), the DRF has the worst lateral resolution ability among the five methods, and it cannot distinguish the neighboring targets. In order to investigate the capabilities of lateral resolution and the sidelobe suppression of the proposed method, the lateral curves at the depth of 85mm is further analyzed. The mainlobe of DRF is the widest, and correspondingly the lateral resolution is worst, AB method is better than DRF. The mainlobe width at -6dB of DFB, DFAB and CARDFB are 0.58mm, 0.46mm and 0.4mm respectively.

### 4.2. Robust Investigation

Since the ultrasound imaging systems are always inevitably interfered by various noises. Figure 5 shows echo signals of short pulse excitation and Chirp-coded excitation polluted by the Gauss white noises, and the SNR is 10dB.

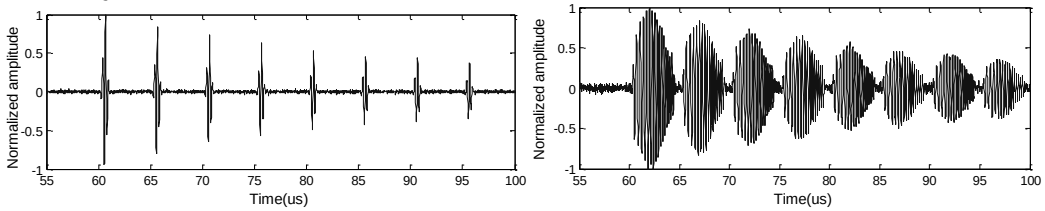


(a) Echo signals of short pulse excitation (b) Echo signals of chirp-coded excitation

**Figure 5. The Comparsion of Noise-polluted Echo Signals between Different Excitation**

Figure 6 shows the images polluted by noises. The quality of all the images are degraded. The DRF almost has no anti-noise capability. AB algorithm has some of anti-noise capacity, however the artifacts is serious. The DFB algorithm has poor anti-noise capability. The DFAB algorithm has better anti-noise performance than DFB. For the CARDFB algorithm with Chirp-code excitation, the noises are sharply restrained by the matched filter and the adaptive weight algorithm, therefore, the quality of the image is greatly improved.

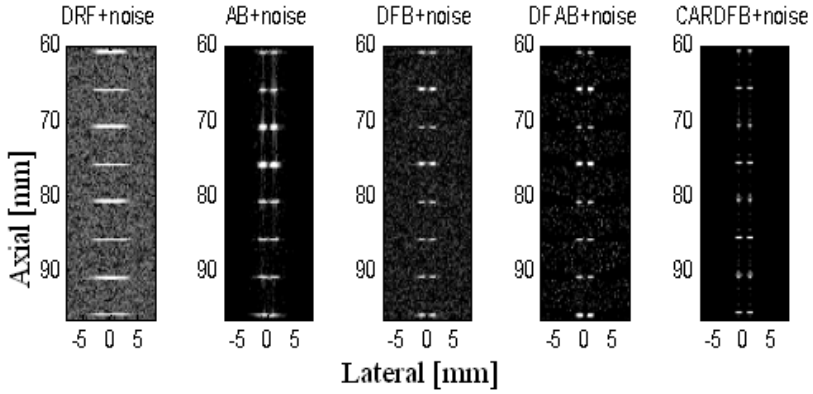


(a) Noise-polluted images of different beamforming methods

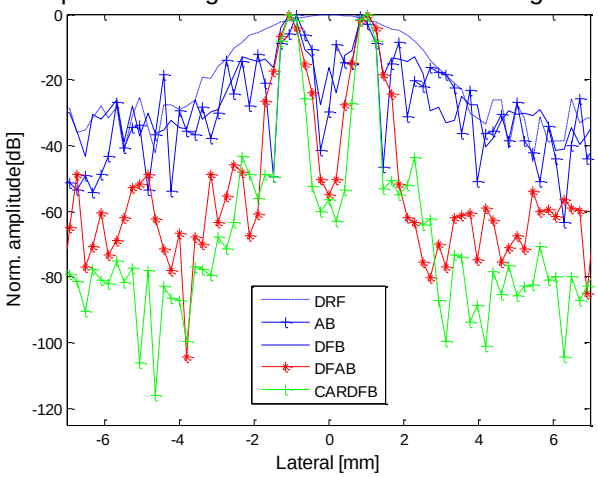


(b) The comparison of lateral curvls at the depth of 85mm with 10dB Gauss White noise

**Figure 6. The Effect of Gauss Noise on Image Reconstruction**

Figure 6 (b) shows the lateral curves of different methods at the depth of 85mm. The main-to-side lobe ratio (MSR) is the amplitude ratio between the mainlobe and the biggest sidelobe. The bigger the MSR is, the more energy the mainlobe concentrates, and correspondingly, the less artifacts and better contrast the image owns. As can be seen from Figure 4 (b) and Figure 6 (b), the MSR with noise-polluted or not can be obtained. The MSR contrast is listed in Table 1. The analyzed axial curve is at the depth of 85mm. For DRF the width of the mainlobe is so wide, the sidelobe is covered. Therefore, the related data of DRF is not listed in Table 1.

**Table 1. MSR Contrast Before and After Adding Noise(Unit: dB)**

| Imaging algorithms | Noise free | Noise polluted | Rate of change |
|---|---|---|---|
| AB | 30 | 13 | 57% |
| DFB | 60 | 12 | 80% |

| | | | |
|---|---|---|---|
| DFAB | 58 | 46 | 21% |
| CARDFB | 82 | 75 | 9% |

From table 1, we can find whether the noises exist or not, the MSR of CARDFB is always the biggest, and the sidelobe is the lowest, which indicates the best performance of robustness against noises.

It should be mentioned that in this paper the duration of Chirp signal is 10us. The impact of the duration of Chirp-coded signal on MSR and detecting depth should be studied in the future.

## 5. Second and Following Pages

In this paper, we propose a new beamforming method CARDFB that fused the advantages of Chirp-coded excitation, adaptive weighting and dual focusing beamform. The scheme can be used in ultrasound imaging. Experimental results indicate that the proposed method can improve the lateral resolution, suppress the sidelobe and strengthen the robustness to noises. The proposed method can provide efficient reference for designing high quality ultrasound imaging system.

## ACKNOWLEDGEMENTS

This work was supported by the Nature Science Founditon of Chongqing City(CSTC2012JJA10129).

## References

[1] T. Yardibi, C. Bahr, N. Zawodny and F. Liu, “Uncertainty analysis of the standard delay-and-sum beamformer and array calibration” im going on vacation, Journal of Sound and Vibration, vol. 329, no. 13, **(2010)**.
[2] M. Klemm, I. J. Craddock, J. A. Leendertz, A. Preece and R. Benjamin, “Improved delay-and-sum beamforming algorithm for breast cancer detection”, International Journal of Antennas and Propagation, **(2008).**
[3] M. O'Donnell, “Coded excitation system for improving the penetration of real-time phased-array imaging systems. Ultrasonics, Ferroelectrics and Frequency Control”, IEEE Transactions on, vol. 39, no. 3, **(1992).**
[4] J. Shen and E. S. Ebbini, “A new coded-excitation ultrasound imaging system. I. Basic principles. Ultrasonics, Ferroelectrics, and Frequency Control”, IEEE Transactions on, vol. 43, no. 1, **(1996)**.
[5] C. H. Frazier and W. D. O'Brien, “Synthetic aperture techniques with a virtual source element. Ultrasonics”, Ferroelectrics and Frequency Control, IEEE Transactions on, vol. 45, no. 1, **(1998)**.
[6] M. H. Bae and M. K. Jeong, “A study of synthetic-aperture imaging with virtual source elements in B-mode ultrasound imaging systems”, Ultrasonics, Ferroelectrics and Frequency Control, IEEE Transactions on, vol. 47, no. 6, **(2000)**.
[7] M. H. Skjelvareid, Y. Birkelund and Y. Larsen, “Internal pipeline inspection using virtual source synthetic aperture ultrasound imaging”, NDT & E International, vol. 54, **(2013)**.
[8] C. H. Chang, Y. F. Chang, Y. Ma and K. K. Shung, “Reliable estimation of virtual source position for SAFT imaging. Ultrasonics, Ferroelectrics and Frequency Control”, IEEE Transactions on, vol. 60, no. 2, **(2013)**.
[9] C. C. Ho, Y. H. Lin and S. H. Wang, “A Modified Synthetic Aperture Focusing Technique Using Beam Characteristics of Transducer for Ultrasound Image Improvement”, The 15th International Conference on Biomedical Engineering, :Singapore, **(2014)** December 4-7.
[10] T. K. Toosi and H. Behnam, “Combined pulse compression and adaptive beamforming in coded excitation ultrasound medical imaging”, 2009 International Conference on Signal Processing Systems, Singapore, **(2009)** May 15-17.
[11] V. Dutt and J. F. Greenleaf, “Adaptive speckle reduction filter for log-compressed B-scan images. Medical Imaging”, IEEE Transactions on, vol. 5, no. 6, **(1996)**.
[12] C. Zheng, H. Peng, W. Zhu and Z. Han, “Synthetic Aperture Ultrasonic Imaging Based on Coded Exciting and Coherence Factor Adaptive Weighting”, Intelligent Computation and Bio-Medical Instrumentation (ICBMI), 2011 International Conference on. IEEE, Wuhan ,China, **(2011)** December 14-17.

 

[13] J. F. Synneva, A. Austeng and S. Holm, "Adaptive beamforming applied to medical ultrasound imaging. Ultrasonics,Ferroelectrics and Frequency Control", IEEE Transactions on, vol. 54, no. 8, **(2007)**.
[14] A. Zoubir and Y. Wang, "Robust generalised Capon algorithm for estimating the angular parameters of multiple incoherently distributed sources", Signal Processing, IET, vol. 2, no. 2, **(2008)**.
[15] B. M. Asl and A. Mahloojifar, "Contrast enhancement and robustness improvement of adaptive ultrasound imaging using forward-backward minimum variance beamforming", Ultrasonics, Ferroelectrics and Frequency Control, IEEE Transactions on, vol. 58, no. 4, **(2011)**.
[16] B. M. Asl and A. Mahloojifar, "Eigenspace-Based minimum variance beamforming applied to medical ultrasound imaging. Ultrasonics, Ferroelectrics and Frequency Control", IEEE Transactions on, vol. 57, no. 11, **(2010)**.
[17] M. C. Hemmsen, J. M. Hansen and J. A. Jensen, "Synthetic aperture sequential beamformation applied to medical imaging. Synthetic Aperture Radar", 2012. EUSAR. 9th European Conference on VDE, Nuremberg, Germany, **(2012)** April 23-26.
[18] J. Kortbek, J. A. Jensen and M. Ø. Jørgensen, "Synthetic aperture sequential beamforming and other beamforming techniques in ultrasound imaging", BK Medical A/SB-K Medical A/S, **(2008)**.
[19] M. C. Hemmsen, "Image processing in medical ultrasound", DTU Electrical Engineering, **(2011)**.
[20] J. A. Jensen, "Users' guide for the Field II program", Technical University of Denmark , **(2001)**.

## Author

**Wang Linhong** was born in 1974. She received her Ph.D. from Chongqing University, China. She is currently an associated professor in Chongqing College of Electronic Engineering. Her research interest is mainly in the area of ultrasonic imaging algorithm, information acquisition and processing and pattern recognition.